Published in final edited form as:
Bioconjug Chem. 2010 January ; 21(1): 14–19. doi:10.1021/bc900438a.

Binding affinity and kinetic analysis of targeted small molecule-modified nanoparticles

Carlos Tassa[†,‡], **Jay L. Duffner**[‡], **Timothy A. Lewis**[‡], **Ralph Weissleder**[†,‡], **Stuart L. Schreiber**[‡,§], **Angela N. Koehler**[‡], and **Stanley Y. Shaw**[†,‡,*]

[†] Center for Systems Biology, Massachusetts General Hospital and Harvard Medical School, Boston, MA

[‡] Broad Institute of Harvard and M.I.T., Cambridge, MA

[§] Howard Hughes Medical Institute, Dept. of Chemistry and Chemical Biology, Harvard University, Cambridge, MA

Abstract

Nanoparticles bearing surface-conjugated targeting ligands are increasingly being explored for a variety of biomedical applications. The multivalent conjugation of targeting ligands on the surface of nanoparticles is presumed to enhance binding to the desired target. However, given the complexities inherent in the interactions of nanoparticle surfaces with proteins, and the structural diversity of nanoparticle scaffolds and targeting ligands, our understanding of how conjugation of targeting ligands affects nanoparticle binding remains incomplete. Here we use surface plasmon resonance (SPR) to directly and quantitatively study the affinity and binding kinetics of nanoparticles that display small molecules conjugated to their surface. We studied the interaction between a single protein target and a structurally related series of targeting ligands whose intrinsic affinity varies over a 4500-fold range, and performed SPR at protein densities that reflect endogenous receptor densities. We report that even weak small molecule targeting ligands can significantly enhance target-specific avidity (by up to 4 orders of magnitude) through multivalent interactions, and also observe a much broader range of kinetic effects than has been previously reported. Quantitative measurement of how the affinity and kinetics of nanoparticle binding vary as a function of different surface conjugations is a rapid, generalizable approach to nanoparticle characterization that can inform the design of nanoparticles for biomedical applications.

Targeted nanoparticles are an exciting class of materials that are undergoing clinical development as diagnostics, molecular imaging probes, and therapeutic delivery vehicles (1). Targeting is typically achieved through the surface display of multiple high affinity ligands, such as antibodies, peptides, or natural products. Multivalent interactions between the nanoparticles and their targets can increase the affinity of target binding (avidity) (2), much as multivalency in Nature facilitates the attachment of pathogens to host cells, or circulating cells to vascular endothelium (3,4). More recently, investigators have used synthetic, non-natural product small molecules as targeting ligands on the surface of nanoparticles (5,6). This approach allows a much more diverse range of chemical matter to be used for targeting, and enables libraries of small molecule-modified nanoparticles to be rapidly screened for the

[*]Corresponding author. Stanley Y. Shaw, Simches Research Center, 185 Cambridge St., Boston, MA 02114, Fax: 617-643-6133, shaw.stanley@mgh.harvard.edu.

Supporting Information Available

Experimental procedures, characterization data, and NMR spectra for all novel compounds, as well as sensorgrams for small molecules and nanoparticles are provided in the Supporting Information.

desired binding properties. Non-natural product small molecules generally have much weaker affinity for their targets (*e.g.*, micromolar K_D), so their use as targeting ligands assumes that multivalent avidity effects will enhance the binding affinity. This notion is supported by the observation that multivalency enhances the avidity as well as recognition specificity of weak interactions between carbohydrates and their protein partners (7–9), and increases the biologic activity of a weakly-binding therapeutic (10). However, given the complexities inherent in interactions of nanoparticle surfaces with proteins (11,12), we sought to develop an approach that could quantitatively describe the binding of a surface-conjugated nanoparticle to its target, and that was sufficiently rapid and generalizable to be widely applicable to the development and characterization of targeted nanoparticles.

Here, we use surface plasmon resonance (SPR) to directly and systematically study the affinity and binding kinetics (13) of nanoparticles that display targeting small molecules conjugated to their surface. To enable direct comparisons, we study a series of structurally related ligands to the same protein, whose intrinsic K_D varies over a 4500-fold range. Importantly, we perform SPR measurements at target protein densities that are comparable to those reported for known cellular targets. These studies demonstrate that even weak small molecule ligands can increase the avidity of nanoparticle target interactions, but also reveal unanticipated effects on binding kinetics. As targeted nanomaterials move towards clinical application, a quantitative understanding of the structure-activity relationships underlying their avidity and kinetics would inform the future design of targeted nanoparticles.

We chose the well-studied interaction between synthetic derivatives of the natural product FK506 and its target protein, FK506-binding protein 12 (FKBP12). A series of structurally related synthetic FK506 analogs possessing K_Ds that range from 24 nM to 110 μM (14) (Scheme 1A) were individually conjugated to a dextranated magnetic nanoparticle (Cross-Linked Iron Oxide, or CLIO) originally developed for MR imaging (15) and biosensor applications (16). This nanoparticle has a diameter of approximately 38 nm in aqueous solutions. We conjugated small molecule ligands to sulfhydryl reactive groups on the nanoparticle using sulfhydryl exchange, and ultraviolet quantitation of the amount of released pyridine-2-thione (**5**) allowed calculation of the average number of small molecules conjugated to each nanoparticle (17) (Scheme 1A). (For ligands of class **1**, our conjugation linkers utilized the same carboxylic acid moiety that has been previously used to modify this class of compounds while preserving their affinity for FKBP12 (18–21).) Nanoparticles with low and high small molecule valency (approximately 3–5 *vs.* 13–18 small molecules per nanoparticle, respectively) were selected for further study; the number of small molecules conjugated per nanoparticle is depicted in parentheses (*e.g.*, **4a(17)** corresponds to particle **4a** with 17 conjugated small molecules).

Binding of small-molecule-conjugated nanoparticles to their target protein is specific, and exquisitely sensitive to the density of protein immobilized onto the SPR sensor chip. Since our target protein is immobilized to the sensor chip as an FKBP12-GST (glutathione S-transferase) fusion protein, we tested nanoparticles for non-specific binding to GST and saw no binding to either unmodified or small-molecule-conjugated nanoparticles (Fig. 1A and 1B). In contrast, at protein densities commonly used for SPR experiments, targeted nanoparticles remain bound to an FKBP12-GST surface (hereafter called an FKBP12 surface) with no appreciable dissociation even after more than 12 minutes (Fig. 1C). At lower protein densities (*e.g.*, 100 response units, corresponding to approximately 1 protein per 648 nm^2), we observe a measurable (but still slow) off-rate that allows calculation of dissociation kinetics (Fig. 1C). Of note, this low protein density is still the same order of magnitude at which physiologically relevant receptors are expressed on cell surfaces. For instance, the HER2 receptor is expressed in SKBR-3 breast cancer cells at a density of ~ 1×10^6 receptors per cell (22); assuming a single-sided disk 15 microns in diameter, this corresponds to a HER2 receptor every 707

nm^2. An analogous calculation for folate receptors on KB cells (~ 2.5×10^6 receptors per cell (23)) corresponds to a receptor every 283 nm^2.

We measured the association rate k_a, dissociation rate k_d, and dissociation constant K_D (k_d/k_a) for the interaction of FKBP12 with each small molecule (**1a** - **1g**), as well as with those same small molecules conjugated to CLIO nanoparticles (**4a** - **4g**) (Scheme 1A). For each experiment, small molecules or nanoparticles were flowed in parallel over a reference sensor bearing GST (see Supporting Information); the minimal signal arising from GST interaction is then subtracted out to yield SPR tracings that reflect specific interactions with FKBP12 (Figures 1D and 1E). Small molecule and nanoparticle sensorgrams were analyzed with a Langmuir 1:1 binding kinetic analysis, using software provided by the instrument manufacturer (Biacore). $K_{D(free)}$ for all free ligands are in excellent agreement with previously published values, ranging from 24 nM to 110 μM (Table 1). By comparison, the conjugated nanoparticles show profound changes in both association and dissociation kinetics, with only the weakest free ligand, compound **1g**, failing to bind FKBP12 when conjugated to a nanoparticle. As expected, k_d for the multivalent nanoparticles are all markedly decreased relative to the corresponding free ligand (up to 3400-fold slower for **4a(17)** *vs*. **1a**). (Dissociation of FKBP12-GST from the surface is negligible during the time course of these experiments; see Supporting Information.) In contrast, k_a for different nanoparticles show widely divergent effects. For instance, nanoparticle **4a(17)** has a 400-fold *slower* k_a compared to the free ligand **1a**, while nanoparticle **4f(20)** has a 39-fold *faster* k_a compared to the free ligand **1f**.

$K_{D(multivalent)}$ (calculated from k_d and k_a) for all of the nanoparticles is in the single digit nanomolar range. To relate $K_{D(multivalent)}$ to $K_{D(free)}$ in cases where the precise number of ligand-target interactions is not known, Whitesides and colleagues defined an enhancement factor β, which increases as the relative affinity of a multivalent interaction increases: $\beta = K_{D(free)}/K_{D(multivalent)}$ (3). For the multivalent nanoparticles tested here, β ranges from approximately 4 to 9500; the largest β is for ligand **1f**, with a K_D of 39 μM as a free ligand and a $K_{D(multivalent)}$ of 4.15 nM as nanoparticle **4f(20)**. Thus, nanoparticles bearing ligands with weak intrinsic affinity demonstrate greater β and increased affinity (avidity).

The rate map in Figure 2 graphically summarizes several features of the data: (i) A series of multivalent nanoparticles, all binding to the same protein target with approximately the same $K_{D(multivalent)}$, can nonetheless display markedly different kinetics; (ii) Conjugating free ligands (open symbols) to form the corresponding multivalent nanoparticles (closed symbols) has dramatically diverse effects on interaction kinetics; $k_{d(multivalent)}$ decreases to a variable extent, and $k_{a(multivalent)}$ can increase, decrease or remain largely unchanged; (iii) Under the tested protein densities, adding more small molecule ligands to each nanoparticle has a modest effect on both kinetics and affinity.

We also extended our analysis to a relatively uncharacterized synthetic small molecule screening "hit". Compound **6** (Scheme 1B), discovered through a biochemical affinity screen, binds aurora A kinase with $K_{D(free)}$ = 4 μM (24). We conjugated **6** to CLIO using sulfhydryl exchange (conjugates **7(14)** and **9(16)**) or Cu(I)-catalyzed Huisgen 1,3-dipolar cycloaddition ("click" chemistry, conjugate **8**) (Scheme 1B). (Conjugation of **6** to CLIO utilized the same primary alcohol that was used to immobilize **6** in the affinity screen that led to its discovery (19, 24).) Nanoparticle **7(14)** does not bind to immobilized aurora A kinase (data not shown). In contrast, nanoparticles **9(16)** (with a similar but longer linker than the inactive **7(14)**) and **8** both show significantly increased avidity, with $K_{D(multivalent)}$ = 9 and 4 nM, and β = 480 and 1100, respectively (Table 1 and Fig. 2). Thus, in this second model system, multivalent attachment of a weakly binding screening "hit" results in large β factors and enhanced avidity towards the compound's target. The rate map in Figure 2 illustrates how different methods of

conjugating the same molecule (*e.g.*, in nanoparticles **9(16)** and **8**) can result in significantly divergent effects on binding kinetics (especially with regard to k_a) (Fig. 2).

Because it is not possible to precisely determine the number of interactions each nanoparticle makes with immobilized ligands, all of the above sensorgrams used a simple binary interaction model (similar to one used for other nanoparticle studies (23); full details in Supporting Information). In fact, a binary model fits the data quite well with very small residual differences (between experimental and fitted curves; residual curves are shown in Supporting Information) and small χ^2 values (minimized sum of the squared residual difference). This is consistent with our choice of relatively sparse protein densities to mimic physiologic receptor densities. To estimate the contribution of higher order interactions, we reanalyzed the data using a tertiary interaction model (*i.e.*, corresponding to a bivalent interaction between the nanoparticle and protein) as follows (the full binding model is described in Supporting Information):

$$A+B \leftrightarrows AB \text{ (with rate constants } k_{a1} \text{ and } k_{d1}, \text{ and } K_{D1}=k_{d1}/k_{a1}) \quad 1)$$

$$AB+B \leftrightarrows AB_2 \text{ (with rate constants } k_{a2} \text{ and } k_{d2}, \text{ and } K_{D2}=k_{d2}/k_{a2}) \quad 2)$$

For the conjugated nanoparticles **4a** – **4f** and **9**, the ratio of K_{D1}/K_{D2} correlates with $K_{D(ligand)}$, the dissociation constant for the free ligand ($R^2 = 0.57$; Table 2 and Fig. 3A). That is, the bivalent mode of binding contributes more to the overall nanoparticle interaction (greater K_{D1}/K_{D2} ratio) for nanoparticles bearing ligands of *weaker* intrinsic affinity (larger $K_{D(ligand)}$). This is consistent with our finding that nanoparticles bearing weaker ligands also exhibit the greatest β and enhancement of avidity. Interestingly, the avidity effect for weaker ligands appears to be mediated primarily by the dissociation rate of the bivalent interaction. The dissociation constant for the free ligand ($K_{D(ligand)}$) shows a strong correlation with k_{d1}/k_{d2} ($R^2 = 0.76$; for weaker free ligands, $k_{d1} \gg k_{d2}$) but no correlation with k_{a1}/k_{a2} ($R^2 = 0.01$) (Table 2 and Figs. 3B and 3C). While it is uncertain whether the nanoparticles interact through bivalent or higher order interactions, this analysis confirms that multivalent interactions make important contributions to nanoparticle avidity.

Predicting the structure-activity relationships (SAR) for multivalent ligands has not been straightforward, even for relatively small systems such as dimers of the antibiotic vancomycin (25). This problem is exacerbated as functionalized nanoparticles increasingly utilize chemically and structurally diverse scaffolds (*e.g.*, dextranated nanoparticles, dendrimers, albumin, liposomes) and targeting ligands (*e.g.*, antibodies, peptides, aptamers or low affinity small molecules). Here, we have performed SPR on relatively sparse but physiologic protein surfaces (22,23) to very sensitively detect how subtle variations in targeting ligands can affect binding kinetics and affinity. Our target protein densities are approximately 100-fold sparser than those used to document very large avidity effects for folate-targeted dendrimers (23), and our findings provide a complementary view of avidity at a distinct, physiologically relevant regime of protein concentrations. Using even slightly denser (*e.g.*, 4-fold) protein surfaces we observed essentially no dissociation of nanoparticles (Fig. 1C), which suggests that our results may underestimate the maximal avidity obtainable with these particles, as well as the contribution of higher ligand valencies. Other factors, such as deformable and fluid membranes that could facilitate close apposition of cellular receptors, could further increase avidity.

We demonstrate strong avidity effects (β of up to 4 orders of magnitude) for nanoparticles conjugated to relatively weak (micromolar K_D) small molecule ligands, including “hits” from a high-throughput screen. We observed a dramatic decrease in k_d for the nanoparticles relative to the free ligand, consistent with other reports (23); however, we observed a much wider

variety of effects on k_a than has been reported previously, including markedly increased, markedly decreased, or unchanged k_a relative to the free ligands. These unanticipated effects on binding kinetics were revealed because of the deliberate constraints of our experiment (a common protein target, shared nanoparticle scaffold, similar valency, and identical conjugation chemistry), which were imposed to allow detailed comparisons of multivalent binding. The kinetic differences displayed by our series of related functionalized nanoparticles could translate into functional differences. For instance, nanoparticle affinity, and association and dissociation rates can all affect how deeply an intravascular circulating agent penetrates into tissue before its target sites become effectively saturated (26); the relative contribution of these variables depends on several *in vivo* factors, including capillary permeability, particle size and target density.

Overall, this approach can be generalized rapidly to a variety of ligand-target combinations, as it does not require *de novo* development of a cell-based assay for each target. Systematic application of this approach could reveal principles that guide nanoparticle design. For instance, our studies suggest that a view in which nanoparticles are largely modular assemblies of scaffold, linker and targeting ligand may be too simplistic; instead, SPR studies could clarify how different structural components collaborate to determine binding kinetics and affinities. Our data also suggest testable hypotheses about how nanoparticles with distinct binding and kinetic properties will behave in complex *in vitro* and *in vivo* systems. This in turn has broad implications for the design and synthesis of functionalized nanoparticles for the imaging, diagnosis and treatment of disease.

Supplementary Material

Refer to Web version on PubMed Central for supplementary material.

Acknowledgments

This work has been supported by the National Institutes of Health, National Heart Lung Blood Institute (HL077186 to S.Y.S., HL80731 to S.Y.S., S.L.S. and R.W) and National Cancer Institute (CA119349 to R.W.); and the Broad Institute of Harvard and MIT (to S.Y.S., R.W. and S.L.S.). The authors acknowledge Dr. Kara Herlihy for SPR support, and Jason Fuller, Katie Doud, Dr. Ralph Mazitschek, Dr. Eric Yi Sun, Dr. Lee Josephson, Dr. Karl Munger and Dr. Hiroyuki Hayakawa for reagents and comments.

LITERATURE CITED

1. De M, Ghosh PS, Rotello VM. Applications of nanoparticles in biology. Adv Mater 2008;20:4225–4241.
2. Montet X, Funovics M, Montet-Abou K, Weissleder R, Josephson L. Multivalent effects of RGD peptides obtained by nanoparticle display. J Med Chem 2006;49:6087–6093. [PubMed: 17004722]
3. Mammen M, Choi SK, Whitesides GM. Polyvalent interactions in biological systems: Implications for design and use of multivalent ligands and inhibitors. Angew Chem Int Ed 1998;37:2754–2794.
4. Mulder A, Huskens J, Reinhoudt DN. Multivalency in supramolecular chemistry and nanofabrication. Org Biomol Chem 2004;2:3409–3424. [PubMed: 15565230]
5. Weissleder R, Kelly K, Sun EY, Shtatland T, Josephson L. Cell-specific targeting of nanoparticles by multivalent attachment of small molecules. Nat Biotechnol 2005;23:1418–1423. [PubMed: 16244656]
6. Kelly KA, Shaw SY, Nahrendorf M, Kristoff K, Aikawa E, Schreiber SL, Clemons PA, Weissleder R. Unbiased discovery of *in vivo* imaging probes through *in vitro* profiling of nanoparticle libraries. Integr Biol 2009;1:311–317.
7. Mortell KH, Weatherman RV, Kiessling LL. Recognition specificity of neoglycopolymers prepared by ring-opening metathesis polymerization. J Am Chem Soc 1996;118:2297–2298.
8. Kiessling LL, Gestwicki JE, Strong LE. Synthetic multivalent ligands in the exploration of cell-surface interactions. Curr Opin Chem Biol 2000;4:696–703. [PubMed: 11102876]

9. Carlson CB, Mowery P, Owen RM, Dykhuizen EC, Kiessling LL. Selective tumor cell targeting using low-affinity, multivalent interactions. ACS Chem Boil 2007;2:119–127.
10. Bowman MC, Ballard TE, Ackerson CJ, Feldheim DL, Margolis DM, Melander C. Inhibition of HIV fusion with multivalent gold nanoparticles. J Am Chem Soc 2008;130:6896–6897. [PubMed: 18473457]
11. Cedervall T, Lynch I, Lindman S, Berggard T, Thulin E, Nilsson H, Dawson KA, Linse S. Understanding the nanoparticle-protein corona using methods to quantify exchange rates and affinities of proteins for nanoparticles. Proc Natl Acad Sci U S A 2007;104:2050–2055. [PubMed: 17267609]
12. Lundqvist M, Stigler J, Elia G, Lynch I, Cedervall T, Dawson KA. Nanoparticle size and surface properties determine the protein corona with possible implications for biological impacts. Proc Natl Acad Sci U S A 2008;105:14265–14270. [PubMed: 18809927]
13. Myszka DG. Kinetic analysis of macromolecular interactions using surface plasmon resonance biosensors. Curr Opin Biotech 1997;8:50–57. [PubMed: 9013659]
14. Keenan T, Yaeger DR, Courage NL, Rollins CT, Pavone ME, Rivera VM, Yang W, Guo T, Amara JF, Clackson T, Gilman M, Holt DA. Synthesis and activity of bivalent FKBP12 ligands for the regulated dimerization of proteins. Bioorg Med Chem 1998;6:1309–1335. [PubMed: 9784872]
15. Nahrendorf M, Jaffer FA, Kelly KA, Sosnovik DE, Aikawa E, Libby P, Weissleder R. Noninvasive vascular cell adhesion molecule-1 imaging identifies inflammatory activation of cells in atherosclerosis. Circulation 2006;114:1504–1511. [PubMed: 17000904]
16. Perez JM, Josephson L, O'Loughlin T, Hogemann D, Weissleder R. Magnetic relaxation switches capable of sensing molecular interactions. Nat Biotechnol 2002;20:816–820. [PubMed: 12134166]
17. Zhao M, Kircher MF, Josephson L, Weissleder R. Differential conjugation of tat peptide to superparamagnetic nanoparticles and its effect on cellular uptake. Bioconjug Chem 2002;13:840–844. [PubMed: 12121140]
18. MacBeath G, Schreiber SL. Printing proteins as microarrays for high-throughput function determination. Science 2000;289:1760–1763. [PubMed: 10976071]
19. Bradner JE, McPherson OM, Mazitschek R, Barnes-Seeman D, Shen JP, Dhaliwal J, Stevenson KE, Duffner JL, Park SB, Neuberg DS, Nghiem P, Schreiber SL, Koehler AN. A robust small-molecule microarray platform for screening cell lysates. Chem Biol 2006;13:493–504. [PubMed: 16720270]
20. Wang X, Imber BS, Schreiber SL. Small-molecule reagents for cellular pull-down experiments. Bioconjug Chem 2008;19:585–587. [PubMed: 18193824]
21. Ong SE, Schenone M, Margolin AA, Li X, Do K, Doud MK, Mani DR, Kuai L, Wang X, Wood JL, Tolliday NJ, Koehler AN, Marcaurelle LA, Golub TR, Gould RJ, Schreiber SL, Carr SA. Identifying the proteins to which small-molecule probes and drugs bind in cells. Proc Natl Acad Sci U S A 2009;106:4617–4622. [PubMed: 19255428]
22. Nielsen UB, Kirpotin DB, Pickering EM, Drummond DC, Marks JD. A novel assay for monitoring internalization of nanocarrier coupled antibodies. BMC Immunol 2006;7:24–38. [PubMed: 17014727]
23. Hong S, Leroueil PR, Majoros IJ, Orr BG, Baker JRJ, Banaszak Holl MM. The binding avidity of a nanoparticle-based multivalent targeted drug delivery platform. Chem Biol 2007;14:107–115. [PubMed: 17254956]
24. Miao H, Tallarico JA, Hayakawa H, Munger K, Duffner JL, Koehler AN, Schreiber SL, Lewis TA. Ring-opening and ring-closing reactions of a shikimic acid-derived substrate leading to diverse small molecules. J Comb Chem 2007;9:245–253. [PubMed: 17348730]
25. Griffin JH, Linsell MS, Nodwell MB, Chen Q, Pace JL, Quast KL, Krause KM, Farrington L, Wu TX, Higgins DL, Jenkins TE, Christensen BG, Judice JK. Multivalent drug design. Synthesis and in vitro analysis of an array of vancomycin dimers. J Am Chem Soc 2003;125:6517–6531. [PubMed: 12785792]
26. Thurber GM, Schmidt MM, Wittrup KD. Factors determining antibody distribution in tumors. Trends Pharmacol Sci 2008;29:57–61. [PubMed: 18179828]

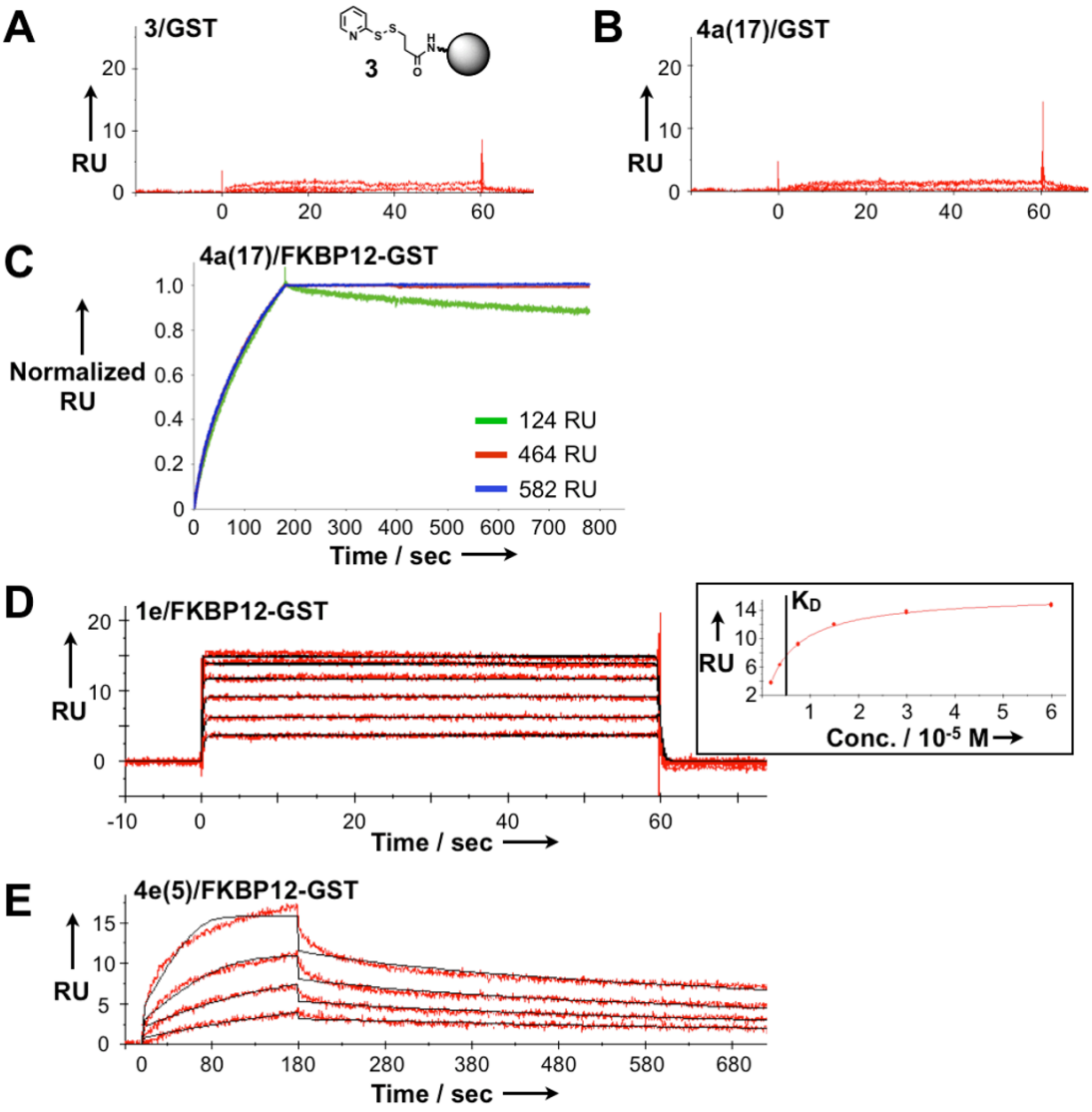

Figure 1.

Specific protein-nanoparticle binding documented in SPR sensorgrams. A. Nanoparticle intermediate **3** does not bind to a control surface of GST. B. Targeted nanoparticle **4a(17)** does not bind to a GST surface. C. Sensorgrams for targeted nanoparticle **4a(17)** at different immobilization densities of FKBP12-GST. Significant binding occurs; appreciable dissociation only occurs at the lowest protein density tested. D. Representative sensorgram for a free small molecule (**1e**) flowed over an FKBP12-GST surface. Inset: Depiction of calculating K_D from steady state affinity studies. E. Representative sensorgram for multivalent nanoparticle **4e(5)**. In figure parts D. and E., red curves depict experimental data at different analyte concentrations; fitted curves modeled to describe a 1:1 binding event are overlaid in black.

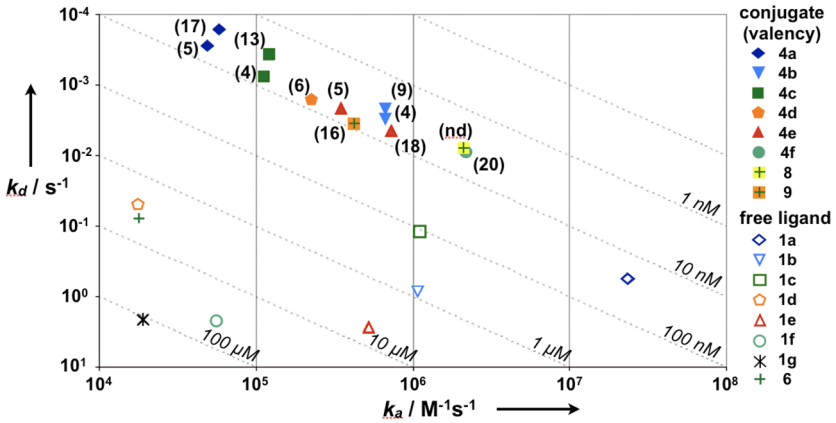

Figure 2.

Rate maps summarizing binding affinity and kinetics. Different combinations of k_a and k_d that result in the same K_D are indicated by dashed lines. Data for free ligands is depicted by open symbols; for each ligand, the corresponding nanoparticles are depicted by a solid symbol of the same shape, with conjugation valency listed in parentheses next to the solid symbol. Valency of **8(nd)** was not determined.

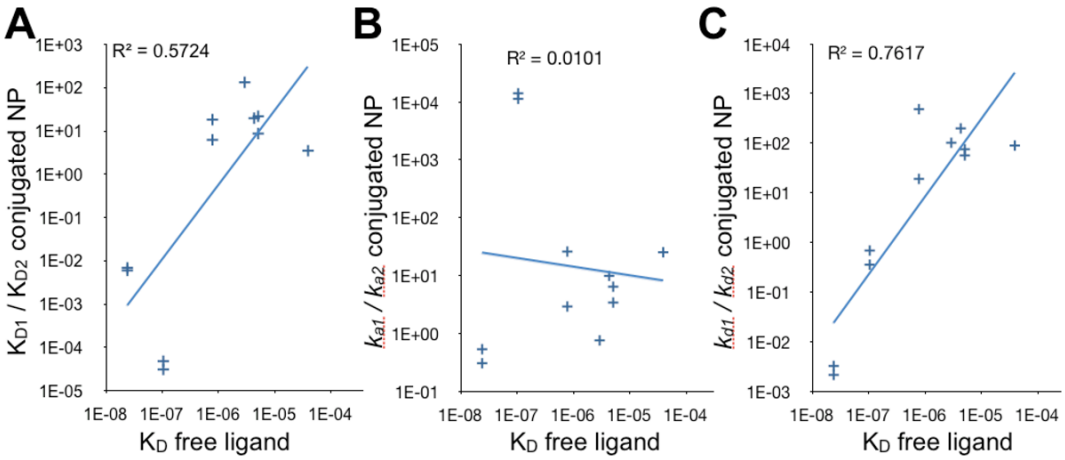

Figure 3.

Relative contribution of monovalent vs. bivalent reaction terms to nanoparticle binding as a function of the intrinsic K_D of the free ligand. A. As the intrinsic affinity of the free ligand becomes weaker, K_{D1}/K_{D2} increases ($R^2 = 0.57$). B. No correlation between k_{a1}/k_{a2} and intrinsic affinity of the free ligand. C. As the intrinsic affinity of the free ligand becomes weaker, k_{d1}/k_{d2} increases ($R^2 = 0.76$).

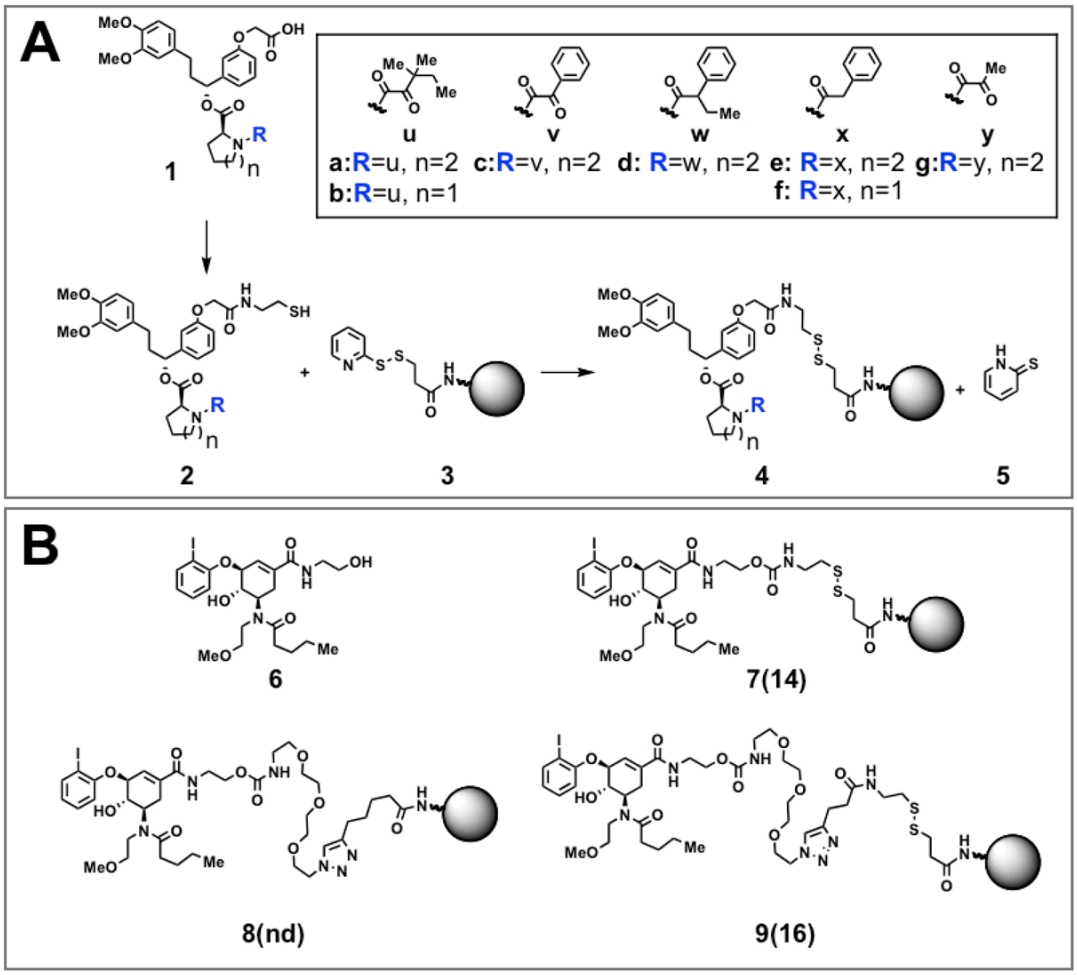

Scheme 1.

Conjugation of small molecules to nanoparticles. A. Conjugation of a series of synthetic derivatives of FK506 (**1**) by sulfhydryl exchange. B. Conjugation of a small molecule that binds aurora A kinase (**6**) by sulfhydryl exchange and Huisgen 1,3-dipolar cycloaddition.

Table 1

Equilibrium affinity and rate constants derived from a Langmuir 1:1 binding kinetic analysis. Corresponding groups of free ligand and conjugated nanoparticles are listed in alphabetical order (**a-g**). Nanoparticle names have the measured number of small molecules conjugated per nanoparticle (valency) in parentheses. $\beta = K_{D(free)}/K_{D(multivalent)}$. Valency was not determined for nanoparticle **8(nd)**.

Analyte (valency)	k_a ($M^{-1}s^{-1}$)	k_d (s^{-1})	K_D (M) multivalent	β	K_D (M) ligand	χ^2 (RU^2)
1a	2.31E+07	0.557	--	--	2.41E-08	0.11
4a(5)	4.88E+04	2.78E-04	5.68E-09	4	--	0.45
4a(17)	5.76E+04	1.64E-04	2.84E-09	8	--	0.60
1b	1.04E+06	0.812	--	--	7.85E-07	0.17
4b(4)	6.64E+05	2.86E-03	4.30E-09	182	--	0.17
4b(9)	6.62E+05	2.08E-03	3.14E-09	250	--	0.40
1c	1.11E+06	0.117	--	--	1.05E-07	0.37
4c(4)	1.13E+05	7.64E-04	6.77E-09	16	--	0.29
4c(13)	1.21E+05	3.58E-04	2.96E-09	36	--	0.33
1d	1.70E+04	0.0500	--	--	2.94E-06	0.29
4d(6)	2.19E+05	1.62E-03	7.39E-09	398	--	0.05
1e	5.23E+05	2.67	--	--	5.11E-06	0.35
4e(5)	3.46E+05	2.15E-03	6.20E-09	824	--	0.19
4e(18)	7.29E+05	4.43E-03	6.09E-09	840	--	0.26
1f	5.62E+04	2.21	--	--	3.94E-05	0.61
4f(20)	2.17E+06	9.01E-03	4.15E-09	9498	--	0.72
1g	1.90E+04	2.08	--	--	1.10E-04	0.58
6	1.79E+04	0.0775	--	--	4.33E-06	0.37
8(nd)	2.13E+06	8.32E-03	3.91E-09	1107	--	0.64
9(16)	4.20E+05	3.82E-03	9.08E-09	477	--	0.58

Table 2

Equilibrium affinity and rate constants derived from a tertiary interaction (bivalent) kinetic analysis. Bivalent interactions between A (analyte) and B (immobilized ligand) are described by the following equations:

Analyte	k_{a1} ($M^{-1}s^{-1}$)	k_{d1} (s^{-1})	k_{a2} ($M^{-1}s^{-1}$)*	k_{d2} (s^{-1})	K_{D1} (M)	K_{D2} (M)	K_{D1}/K_{D2}	χ^2 (RU^2)
4a(5)	2.61E+04	3.41E-04	4.88E+04	0.106	1.31E-08	2.17E-06	6.03E-03	0.40
4a(17)	3.15E+04	2.31E-04	1.03E+05	0.109	7.33E-09	1.06E-06	6.91E-03	0.44
4b(4)	7.88E+04	2.33E-02	2.70E+04	1.23E-03	2.95E-07	4.69E-08	6.28E+00	0.08
4b(9)	2.17E+05	3.09E-03	8.35E+03	6.43E-06	1.42E-08	7.70E-10	1.84E+01	0.3
4c(4)	2.95E+04	7.99E-04	2.09E+00	1.174E-03	2.71E-08	5.62E-04	4.82E-05	0.37
4c(13)	5.95E+04	3.67E-04	5.26E+00	1.04E-03	6.16E-09	1.98E-04	3.11E-05	0.35
4d(6)	6.1E+04	3.98E-02	8.05E+04	3.92E-04	6.52E-07	4.87E-09	1.33E+02	0.05
4e(5)	2.24E+04	3.49E-02	6.55E+03	4.64E-04	1.56E-06	7.08E-08	2.20E+01	0.08
4e(18)	4.66E+04	3.91E-02	7.26E+03	6.93E-04	8.39E-07	9.55E-08	8.78E+00	0.11
4f(20)	1.62E+05	1.56E-01	6.41E+03	1.75E-03	9.63E-07	2.73E-07	3.52E+00	0.27
9(16)	1.89E+04	2.57E-03	1.91E+03	1.3E-05	1.36E-07	6.84E-09	1.99E+01	0.34

*k_{a2} ($RU^{-1}s^{-1}$) was converted approximately to k_{a2} ($M^{-1}s^{-1}$) as follows: k_{a2} ($M^{-1}s^{-1}$) = k_{a2} ($RU^{-1}s^{-1}$) × MW × 100.

$$A+B \leftrightarrows AB \text{ (with rate constants } k_{a1} \text{ and } k_{d1}, \text{ and } K_{D1}=k_{d1}/k_{a1}) \quad 1)$$

$$AB+B \leftrightarrows AB_2 \text{ (with rate constants } k_{a2} \text{ and } k_{d2}, \text{ and } K_{D2}=k_{d2}/k_{a2}) \quad 2)$$